ISSN 0915 633X

NIFS--494

NATIONAL INSTITUTE FOR FUSION SCIENCE

Tilt Stabilization by Energetic Ions Crossing Magnetic Separatrix in Field-Reversed Configuration

K. Nishimura, R. Horiuchi and T. Sato

(Received - May 6, 1997)

NIFS-494 June 1997

RESEARCH REPORT
NIFS Series

NAGOYA, JAPAN

TILT STABILIZATION BY ENERGETIC IONS CROSSING MAGNETIC SEPARATRIX IN A FIELD-REVERSED CONFIGURATION

Kazumi Nishimura[1], Ritoku Horiuchi[1,2], Tetsuya Sato[1,2]

[1]Department of Fusion Science, The Graduate University for Advanced Studies, Toki 509-52, Japan

[2]Theory and Computer Simulation Center, National Institute for Fusion Science, Toki 509-52, Japan

Abstract

The stabilization of the tilt disruption in a field-reversed configuration is investigated by means of a three-dimensional particle simulation. The growth rate of tilting instability decreases as the β value at magnetic separatrix β_{sp} increases, while it is slightly affected by the finite-Larmor radius parameter $\bar{s}$ and the hollowness parameter of an equilibrium current profile D under the condition that β_{sp} is less than 0.1. It is found that the number flux of ions crossing the separatrix repeatedly increases with increasing β_{sp} and the crossing motion of energetic ions plays a role in leading to the tilt stabilization by disturbing the unstable tilting motion.

Keywords; field-reversed configuration, FRC, tilt instability, particle simulation

I. Introduction

The tilt instability is one of the global instabilities which lead to the disruption of a FRC (field-reversed configuration) plasma. It has been well-known that a Spheromak is unstable against the tilt instability from the theoretical analysis based on the ideal magnetohydrodynamic (MHD) theory.[1] Compared with the Spheromak, there are a few different features in the FRC, e.g., the FRC plasma is confined only by the poloidal magnetic field and has a finite pressure gradient within the separatrix. The extended analyses concerned with the tilt instability were applied to the FRC and concluded that the tilt mode of the FRC would be also unstable within the framework of ideal MHD theory.[2,3] Although the growth time of this mode was theoretically estimated to be about an Alfvén transit time, experimental observations show that the FRC plasma remains stable for many growth time.[4,5]

Until now, many theoretical and numerical studies have been carried out in order to explain this contradiction and several models have been proposed as a stabilization mechanism against the tilt instability. We particularly notice three effects among them : (A) the finite ion Larmor radius effect, (B) the profile control effect, and (C) the ion beam effect. The finite-Larmor radius effect is characterized by the parameter $\bar{s}$ which is defined by

$$\bar{s} = \int_R^{r_s} r dr / r_s \lambda_i, \tag{1}$$

where r_s is the separatrix radius, R is the radius of the field-null, and λ_i is the local ion gyroradius. It has been numerically evaluated that the growth rate of the tilt mode decreases with decreasing $\bar{s}$.[6,7] The dependence of the tilt instability on $\bar{s}$ can be shown in a recent experimental result. Tuszewski *et al.*[8] have observed the tilt instability for large $\bar{s}$ ($\bar{s} > 2$) in the FRX-C/LSM device. On the other hand, Slough and Hoffman[9] have reported that the tilt mode is stable over a wide range of $\bar{s}$ ($1 < \bar{s} < 8$) in the LSX device. This apparent contradiction between two experimental results means that the tilt

stability is not determined only by a single parameter $\bar{s}$. Second, a possibility to stabilize the tilt mode by controlling an equilibrium profile has been reported.[10,11,12] Cobb *et al.*[10] have pointed out that a FRC with a hollow current profile is stable for the enough high separatrix β value. The ion beam effect or the ion inertia effect can stabilize the tilt mode if its kinetic energy becomes comparable to the bulk plasma energy.[13] However, this effect may be classified into a different category from previous two effects, because it is introduced not to explain the contradiction between theoretical predictions and experimental results, but to apply an additional kinetic effect to the unstable FRC. In this paper, we discuss both the finite ion Larmor radius effect and the profile control effect.

In real plasma various effects are included simultaneously, which makes the phenomena complex. In considering the problem "what is a dominant process leading to the stabilization of the FRC plasma", it is important to develop the physical model which can control each effect independently and dealt with them simultaneously. We carry out the three-dimensional macroscale particle simulation[7] based on such a physical model.

In this paper, we examine the dependences of tilt instability on both the finite ion Larmor radius effect and the profile control effect, and clarify the physical mechanism of tilt stabilization. The simulation model and the initial condition are described in Sec. II. The results obtained from the particle simulation are discussed in Sec. III. We present the stabilization mechanism in connection with the number flux of ions which cross the magnetic separatrix repeatedly in Sec. IV. Summary and discussions are given in Sec. V.

II. Simulation model

We consider the FRC plasma confined by the external magnetic field within the cylindrical conducting vessel. The plasma consists of ions and electrons which are treated as superparticles. The total number of particles is fixed to 10^6. The boundary conditions applied to the vessel surface are the conducting wall in the radial direction ($r = R_d$; R_d

is the vessel radius) and periodic in the axial direction ($z = \pm Z_d$; Z_d is fixed to $3R_d$ in this paper). The equations to be solved are the equations of motion

$$\frac{d(\gamma_j \mathbf{v}_j)}{dt} = \frac{q_j}{m_j}\left[\mathbf{E} + \frac{\mathbf{v}_j}{c}\times\mathbf{B}\right], \tag{2}$$

$$\frac{d\mathbf{x}_j}{dt} = \mathbf{v}_j, \tag{3}$$

and the Maxwell equations

$$\frac{1}{c}\frac{\partial \mathbf{B}}{\partial t} = -\nabla\times\mathbf{E}, \tag{4}$$

$$\frac{1}{c}\frac{\partial \mathbf{E}}{\partial t} = \nabla\times\mathbf{B} - 4\pi\mathbf{j}, \tag{5}$$

$$\nabla\cdot\mathbf{E} = 4\pi\rho, \tag{6}$$

where $\mathbf{x}_j(t), \mathbf{v}_j(t)$, m_j and q_j are the position, the velocity, the rest mass and the charge of the j-th particle, and the relativistic γ-factor of the j-th particle is defined by

$$\gamma_j = 1/\sqrt{1-(\mathbf{v}_j\cdot\mathbf{v}_j)/c^2}. \tag{7}$$

The current density $\mathbf{j}(\mathbf{x},\mathbf{t})$ and the charge density $\rho(\mathbf{x},t)$ are obtained by summing over all the particles, namely,

$$\mathbf{j}(\mathbf{x},\mathbf{t}) = \sum_{j=1}^{N} \frac{q_j \mathbf{v}_j(t)}{c}\, S(\mathbf{x}-\mathbf{x}_j(t)), \tag{8}$$

$$\rho(\mathbf{x},t) = \sum_{j=1}^{N} q_j\, S(\mathbf{x}-\mathbf{x}_j(t)), \tag{9}$$

where N is the total number of particles and $S(\mathbf{x})$ is the form function of particles.[14] The numerical scheme used for the three-dimensional particle simulation relies on the semi-implicit method.[7]

Two-dimensional MHD equilibrium configurations are used for the initial conditions. The pressure profile $P(\Psi)$ is written in the form as[10]

$$P(\Psi) = \begin{cases} P_0(K_0 - \chi - \frac{1}{2}D\chi^2) & \text{for } \chi \le 0 \\ P_0 K_0 e^{-\chi/K_0} & \text{for } \chi > 0, \end{cases} \tag{10}$$

where Ψ denotes the poloidal flux function, $\chi = \Psi/|\Psi_{ax}|$, Ψ_{ax} is the Ψ value at the field null, P_0 is constant, $K_0 = \beta_{sp}(1-D/2)/(1-\beta_{sp})$, $\beta_{sp}(= P(0)/P(\chi = 1))$ is the normalized pressure value at the magnetic separatrix, and D is hollowness parameter. The parameter β_{sp} represents roughly the plasma β value at the separatrix for the FRC plasma. This form of the pressure profile is equal to that used in neither Barnes *et al.*[6] nor Horiuchi and Sato.[7] Two-dimensional MHD equilibrium as the initial condition is obtained by an iteration method[15] for solving the Grad-Shafranov equation. The ion temperature and the electron temperature are assumed to be the same and spatially uniform. Then the initial positions and velocities of particles are determined through the pressure $P(\boldsymbol{r}, t)$, number density n($\boldsymbol{r}$,t) and diamagnetic current $\boldsymbol{J}(\boldsymbol{r}, t)$ by using the quiet-start technique.[16]

The parameters used for the simulation are listed in Table I. In the present model, three parameters can be controlled independently. The first is the parameter $\bar{s}$ which controls the finite-Larmor radius effect. The others are the profile control parameters β_{sp} and D which determine the value of the pressure at the separatrix, and the hollowness of the current profile, respectively.

III. Simulation results

Let us examine the behaviors of the tilt instability based on the simulation results for the typical case R1. Figures 1 and 2 depict the spatial profiles of mass flow vectors and mass density contours in the (r,z) plane at four different time periods, respectively. Time is normalized by the Alfvén transit time $t_A(= R_d/V_A)$ where V_A is Alfvén velocity estimated from the magnetic field at $r = R_d$ on the midplane and the ion density at the field-null. It is clearly seen in Fig.1 that the asymmetric flow with respect to the major axis grows gradually as time goes on. As a result of the development of the tilt motion, the two peaks of the density contours move in the opposite directions to each other. The development of tilt instability is hereafter expressed in terms of the Fourier amplitude of

the z-component of the fluid velocity $V_z^{(1)}(t)$, where superscript (1) denotes the azimuthal mode number $n = 1$, the other spatial dependence disappears by integrating it over the (r, z) space.

Three kinds of simulation runs are carried out to investigate the dependence of the tilt instability on the parameter $\bar{s}$, β_{sp}, and D. First, let us examine the dependence on β_{sp}. Figure 3 shows the time histories of tilt mode $V_z^{(1)}$ for three different values of β_{sp} where $\bar{s} = 3.0$, $D = -0.6$ and β_{sp} are 0.02 (R1), 0.10 (R2), and 0.20 (R3), respectively. The growth rate γ normalized by MHD growth rate γ_M [17,18] is listed in Table I where γ_M is defined by

$$\gamma_M = C\frac{\tilde{V}_A}{Z_{sp}}, \tag{11}$$

$\tilde{V}_A$ is the average Alfvén velocity associated with the volume-averaged magnetic field and the ion density at the field-null, and Z_{sp} is the separatrix half-length in the axial direction. The coefficient C in Eq.(11), which is of the order of unity and depends on the configuration of magnetic separatrix, is fixed to 3 in this paper.[18] Figure 3 clearly shows that the growth rate decreases drastically with increasing β_{sp}. For the case of $\beta_{sp} = 0.02$, it can be found that the tilt mode is fairly unstable in comparison with the other cases of $\beta_{sp} = 0.10$ and 0.20.

Now let us examine how the tilt instability is affected by the finite-Larmor radius effect. The time histories of the tilt modes are shown in Fig.4 for three different values of $\bar{s}$ where $\beta_{sp}(= 0.02)$ and $D(= -0.6)$ are fixed, the values of $\bar{s}$ are equal to 2.0 (R4), 3.0 (R1), and 5.0 (R5), respectively. There are no distinct differences among the growth rates (also see the cases R1, R4, R5 in Table I). The previous simulation results[6,7] indicated that the growth rate of tilt mode decreases with decreasing $\bar{s}$. The differences between the previous and our results may be explained by following reasons. Horiuchi *et al.*[7] expressed the FRC plasma by the rigid rotor model in which average ion velocity along the θ direction increases as the radial location moves outwards and $\bar{s}$ decreases. Thus,

the stabilization by the ions with a high rotational velocity may be more efficient with decreasing $\bar{s}$. Furthermore, their initial condition was fairly different from that of the present model, e.g., the pressure profile $P(\Psi)$.

In Fig.5, time histories of the tilt mode are shown for three cases with the different hollowness parameters where $\beta_{sp}(= 0.10)$ and $\bar{s}(= 3.0)$ are fixed, the values of D are -0.6 (R2), 0.0 (R9), and 0.4 (R7). Cobb *et al.*[10] showed that the tilt mode tends to be stable if β_{sp} is enough large and the current profile is hollow. We can not find such a tendency in the behavior of the growth rate, as is shown in Fig.5. The reason may come from the fact that the value of β_{sp} $(= 0.1)$ used here is too small compared with that $(= 0.6)$ in Cobb *et al.*

These results lead us to the conclusion that both the finite-Larmor radius effect (parameter $\bar{s}$) and the profile control effect (hollowness parameter D) are not efficient in the FRC plasma of small β_{sp}, but the tilt stabilization effect becomes significant only in the large β_{sp} plasma.

IV. Stabilization mechanism

In order to clarify the stabilization mechanism by the parameter β_{sp}, we focus on the role of the ions which move across the separatrix repeatedly (we call them "cycling ions" to distinguish them from the diffusive ions). The number of the cycling ions can be calculated each Alfvén time (cycling ion flux). The time histories of cycling ion flux are shown in Fig.6 for the same cases as Fig.3 where the ion flux is normalized by the initial total number of ions. The number flux increases monotonously with increasing β_{sp}. At the period of $t/t_A = 2$, the flux becomes equal to 1.2×10^{-1} for $\beta_{sp} = 0.02$, 2.4×10^{-1} for $\beta_{sp} = 0.1$, and $4.3 \times 10^{-1}$for $\beta_{sp} = 0.2$, respectively. In contrast to this, the number flux scarcely depends on the values of $\bar{s}$ and D, as is seen in Figs.7 and 8. That is, the flux increases slightly as $\bar{s}$ decreases (see Fig. 7) or the current profile becomes hollow

(see Fig. 8). However, the net increments in the flux for both cases are much smaller compared with that in Fig.6. Figure 9 shows the growth rate as a function of the averaged flux of cycling ions per Alfvén time for all cases from R1 to R10 in Table I. It is important to note that there is a clear correlation between the averaged flux and growth rates of the tilt mode i.e., the larger the averaged flux is, the smaller the growth rate becomes. In other words, energetic ions crossing the magnetic separatrix repeatedly contribute to the stabilization of the tilt mode.

In order to elucidate the physical picture of the tilt stabilization by the cycling ions, let us expand the current density into the cycling component $\mathbf{J}^{(c)}$ and the non-cycling component $\mathbf{J}^{(n)}$. The force $(\mathbf{J} \times \mathbf{B})_z^{(1)}$ which generates the tilt motion in the plasma can be calculated with these two components separately. Suppose that Fourier expansion of the force takes the following form as

$$(\mathbf{J}^{(\alpha)} \times \mathbf{B})_z^{(1)} = A^{(\alpha)}(r,z)\cos\theta + B^{(\alpha)}(r,z)\sin\theta, \qquad \alpha = c, n. \tag{12}$$

We can define the average amplitude of this force $F^{(\alpha)}(t)$ and the phase difference $\Delta\phi$ between the forces acting on the cycling ions and on the non-cycling ions as

$$F^{(\alpha)}(t) = \sqrt{\langle A^{(\alpha)}\rangle^2 + \langle B^{(\alpha)}\rangle^2}, \qquad \alpha = c, n\ , \tag{13}$$

$$\Delta\phi = \tan^{-1}\frac{\langle B^{(n)}\rangle}{\langle A^{(n)}\rangle} - \tan^{-1}\frac{\langle B^{(c)}\rangle}{\langle A^{(c)}\rangle}, \tag{14}$$

where $\langle\rangle$ stands for the average over the (r,z) space, i.e., $\langle A(r,z)\rangle = \int A(r,z) r dr dz$. Figure 10 shows the time development of (a) the amplitude and (b) the phase difference for the unstable case R4 where the dotted and solid lines represent the forces acting on the cycling ions and the non-cycling ions, respectively. The phase difference is nearly equal to $-\pi$ at $t = 0$ i.e., the directions of two forces are opposite to each other. The difference, however, disappears as time elapses. Thus, one component of the $\mathbf{J} \times \mathbf{B}$ force works synchronously on the plasma to the same direction as the other component so that the tilt instability grows swiftly on the whole. Figure 11 also shows the time development

of (a) the amplitude and (b) the phase difference for the stable case R7. In contrast to the unstable case, the phase difference remains large ($\Delta\phi \sim \pm\pi$), as is seen in Fig.11(b). If we take into account the fact that two forces have always the same amplitude (see Fig.11(a)), it is concluded that the $\mathbf{J} \times \mathbf{B}$ force by the cycling ions works on the plasma so as to cancel the tilting force by the non-cycling ions.

V. Summary and discussions

In order to investigate the tilt stabilization mechanism in the FRC plasma, we have developed a three-dimensional particle simulation code which can describe both the finite ion Larmor radius effect and the profile control effect. By carrying out the simulation runs with different values of β_{sp}, $\bar{s}$ and D, we have clarified that it is effective against the tilt instability to increase the separatrix beta value (β_{sp}). On the other hand, decreasing $\bar{s}$ value and making current profile hollow ($D < 0$) scarcely affect the stabilization of tilt mode under the condition that β_{sp} is less than 0.1. The detailed analysis reveals that the large value of β_{sp} corresponds to the large flux of the ions which cross the magnetic separatrix repeatedly ("cycling" ions). If we choose the suitable profile for ions to be able to cross the separatrix many times, the growth rate of the tilt mode can be reduced.

After all, the cycling ions are found to contribute to the suppression of the tilt instability. The stabilization mechanism is as follows. Tilt instability is triggered by the internal mode, i.e., the collective motion of plasma is generated inside the magnetic separatrix. The ions which make a cyclic motion across the separatrix are not able to follow the collective motion when they are moving outside of the separatrix. Hence, the phase of cycling ions do not coincide with that of non-cycling ions inside the separatrix. When the cycling ions turn back inside the separatrix, the internal tilting motion is disturbed and suppressed through the interference by the cycling motion. We have confirmed this process by examining the behaviors of two kinds of the tilt forces $(\mathbf{J} \times \mathbf{B})_z^{(1)}$, which act on

the cycling and non-cycling ions. One can speculate that the cycling ions play a role as "chain" to connect the internal plasma and the external plasma and stabilize the tilting motion through their "chain" effect.

Let us discuss the role of electric field. The electric force $qE_z^{(1)}$ may also drive the tilting motion. The difference between the ion and electron Larmor radii causes the charge separation near the separatrix, thus generating the radial components of electric field. However, the radial component causes merely the $\mathbf{E} \times \mathbf{B}$ drift which makes the FRC plasma to rotate about the symmetric axis. It has been observed that the z component E_z which directly cause the tilting motion is always much smaller than the radial component E_r, and the tilting motion is caused by the $\mathbf{J} \times \mathbf{B}$ force, but not by the electric force $q\mathbf{E}$. The same situation holds for the pressure gradient force.

Though the dependence of the tilt mode on $\bar{s}$ value has been observed in some experiment,[8] it is not straightforward to compare experimental results with our simulation results. For example, the experimental equilibrium doesn't coincide with our model exactly and in experiments β_{sp} may be larger than the value of this case ($\beta_{sp} = 0.02$). Moreover, the observed FRC plasma have a tendency to rotate about the symmetric axis which gives rise to the rotational instability.[4] In our equilibrium model, plasma is at rest initially.

Although we have investigated in this paper the system including both the finite-Larmor radius effect and the profile control effect, our model is able to treat the ion beam effect simultaneously with them. That is to say, it is possible to control three kinds of parameters that characterized three effects in the stabilization of tilt mode. This extended study will be reported elsewhere in the future.

Acknowledgments

The simulation work was performed by employing the Advanced Computing System for Complexity Simulation at the National Institute for Fusion Science (NIFS).

This work was supported in part by a Grant-in-Aid from the Ministry of Education, Science and Culture in Japan (No. 07832024, No. 08044109 and No. 08226104).

References

[1]W. N. Rosenbluth, and M. N. Bussac, Nucl. Fusion **19**, 489 (1979).

[2]J. H. Hammer, Nucl. Fusion **21**, 488 (1981).

[3]R. A. Clemente and J. L. Milovich, Phys. Letters **85A**, 148 (1981).

[4]M. Tuszewski, Nucl. Fusion **28**, 2033 (1988).

[5]J. T. Slough and A. L. Hoffman, Nucl. Fusion **28**, 1121 (1988).

[6]D. C. Barnes, J. L. Schwarzmeier, R. Lewis, and C. E. Seyler, Phys. Fluids **29**, 2616 (1986).

[7]R. Horiuchi and T. Sato, Phys. Fluids **B 2**, 2652 (1990).

[8]M. Tuszewski, D. P. Taggart, R. E. Chrien, D. J. Rej, R. E. Siemon, and B. L. Wright, Phys. Fluids **B 3**, 2856 (1991).

[9]J. T. Slough and A. L. Hoffman, Phys. Fluids **B 5**, 4366 (1993).

[10]J. W. Cobb, T. Tajima, and D. C. Barnes, Phys. Fluids **B 5**, 3227 (1993).

[11]L. C. Steinhauer and A. Ishida, Phys. Fluids **B 4**, 645 (1992).

[12]R. Kanno, A. Ishida, and L. C. Steinhauer, J. Phys. Soc. Jpn. **64**, 463 (1995).

[13]D. C. Barnes and R. D. Milroy, Phys. Fluids **B 3**, 2609 (1991).

[14]C. K. Birdsall and A. B. Langdon, *Plasma Physics Via Computer Simulation* (McGraw-Hill, New York, 1985), p. 168.

[15]J. L. Johnson, H. E. Dalhed, J. M. Greene, R. C. Grimm, Y. Y. Hsieh, S. C. Jardin, J. Manickam, M. Okabayashi, R. G. Storer, A. M. M. Todd, D. E. Voss, and K. E. Weimer, J. Comput. Phys. **32**, 212 (1979).

[16]See Ref. 14, p. 36.

[17]J. L. Schwarzmeier, D. C. Barnes, D. W. Hewett, C. E. Seyler, A. I. Shestakov, and R. L. Spencer, Phys. Fluids **26**, 1295 (1983).

[18]R. Horiuchi and T. Sato, Phys. Fluids **B 1**, 581 (1989).

RUN	β_{sp}	D	$\bar{s}$	X_s	E	I_{tot}	γ/γ_M
R1	0.02	−0.6	3.0	0.841	2.14	8.90	0.58
R2	0.10	−0.6	3.0	0.798	2.27	7.20	0.20
R3	0.20	−0.6	3.0	0.739	2.44	6.00	0.02
R4	0.02	−0.6	2.0	0.841	2.14	8.90	1.00
R5	0.02	−0.6	5.0	0.841	2.14	8.90	0.93
R6	0.02	0.4	3.0	0.742	2.46	6.90	0.63
R7	0.10	0.4	3.0	0.709	2.53	6.20	0.33
R8	0.02	0.0	3.0	0.802	2.26	7.90	0.54
R9	0.10	0.0	3.0	0.760	2.39	6.80	0.21
R10	0.02	0.4	2.0	0.742	2.46	6.90	0.70

Table I. Characteristics of equilibrium solutions used in particle simulations, including beta value at separatrix, β_{sp}; hollowness parameter, D; kinetic effect parameter, $\bar{s}$; ratio of separatrix to vessel radius, X_s; elongation, E; total toroidal current, I_{tot}; normalized growth rate, γ/γ_M.

Figure captions

Fig. 1. Vector plots of mass density flux in the (r,z) plane at the periods of $t/t_A = 0.0, 1.0, 3.0, 5.0$ for the case R1.

Fig. 2. Contour plots of mass density for the same case as Fig.1.

Fig. 3. Time history of the tilt mode amplitude $V_z^{(1)}$ for three different values of β_{sp}, i.e., 0.02(R1), 0.10(R2), and 0.20(R3).

Fig. 4. Time history of the tilt mode amplitude $V_z^{(1)}$ for three different values of $\bar{s}$, i.e., 2.0(R4), 3.0(R1), and 5.0(R5).

Fig. 5. Time history of the tilt mode amplitude $V_z^{(1)}$ for three different values of D, i.e., -0.6(R2), 0.0(R9), and 0.4(R7).

Fig. 6. Time history of the normalized flux of the cycling ions per Alfvén time for the same cases as Fig. 3.

Fig. 7. Time history of the normalized flux of the cycling ions per Alfvén time for the same cases as Fig. 4.

Fig. 8. Time history of the normalized flux of the cycling ions per Alfvén time for the same cases as Fig. 5.

Fig. 9. Tilt growth rates as a function of averaged flux of the cycling ions per Alfvén time.

Fig. 10. (a) Time history of tilt force $(\mathbf{J} \times \mathbf{B})_z^{(1)}$ acting on the cycling ion current and the non-cycling ions for the case R4. (b) Time history of phase difference between the tilt force acting on the cycling ion current and that acting on the non-cycling ion current for the same case as Fig. 10(a).

Fig. 11. (a) Time history of tilt force $(\mathbf{J} \times \mathbf{B})_z^{(1)}$ acting on the cycling ion current and the non-cycling ions for the case R7. (b) Time history of phase difference between the

tilt force acting on the cycling ion current and that acting on the non-cycling ion current for the same case as Fig. 11(a).

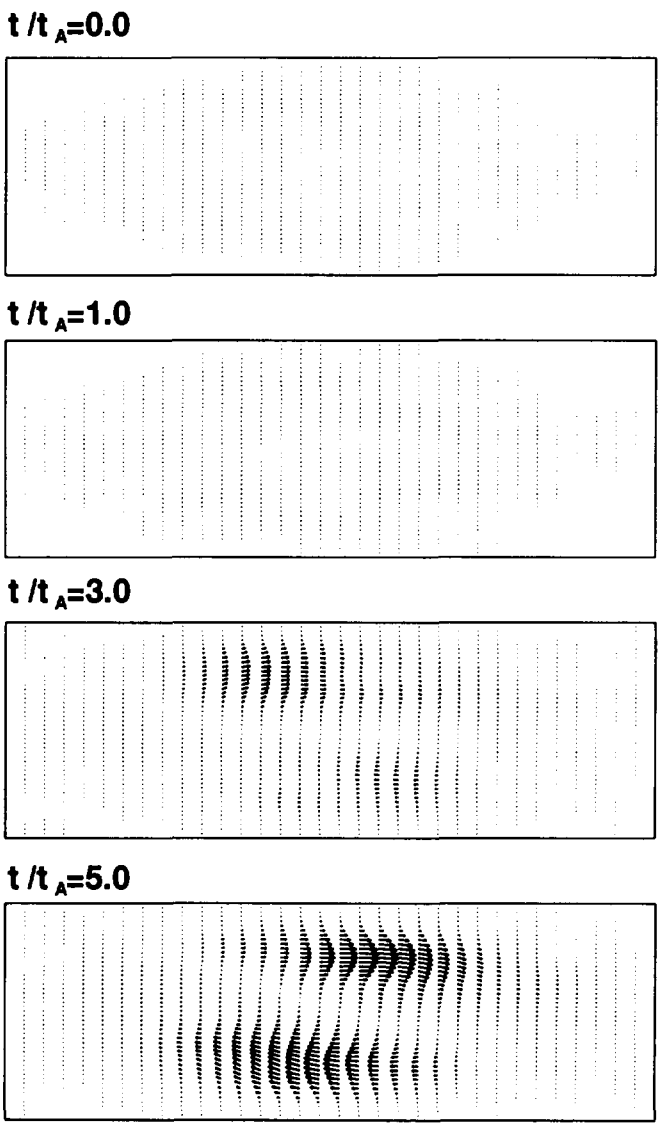

Fig.1

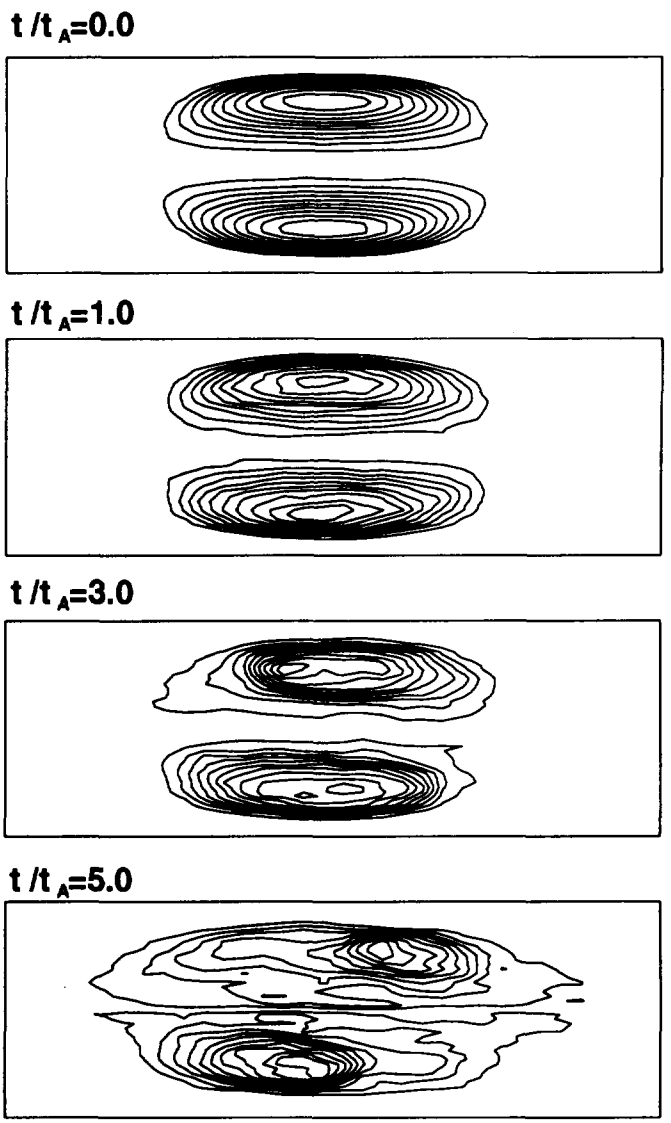

Fig.2

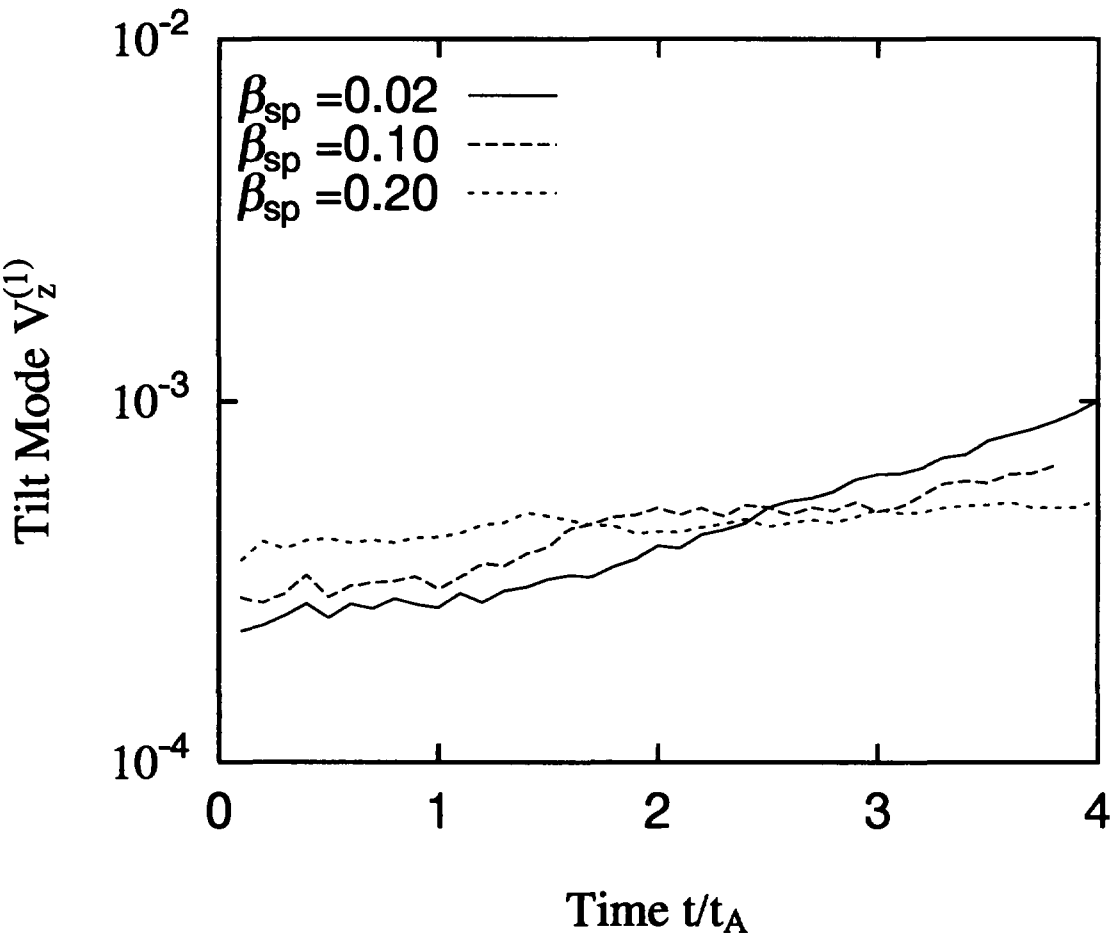
10^{-2}
10^{-3}
10^{-4}
β_{sp} =0.02
β_{sp} =0.10
β_{sp} =0.20
Tilt Mode $V_z^{(1)}$
0
1
2
3
4
Time t/t_A

Fig.3

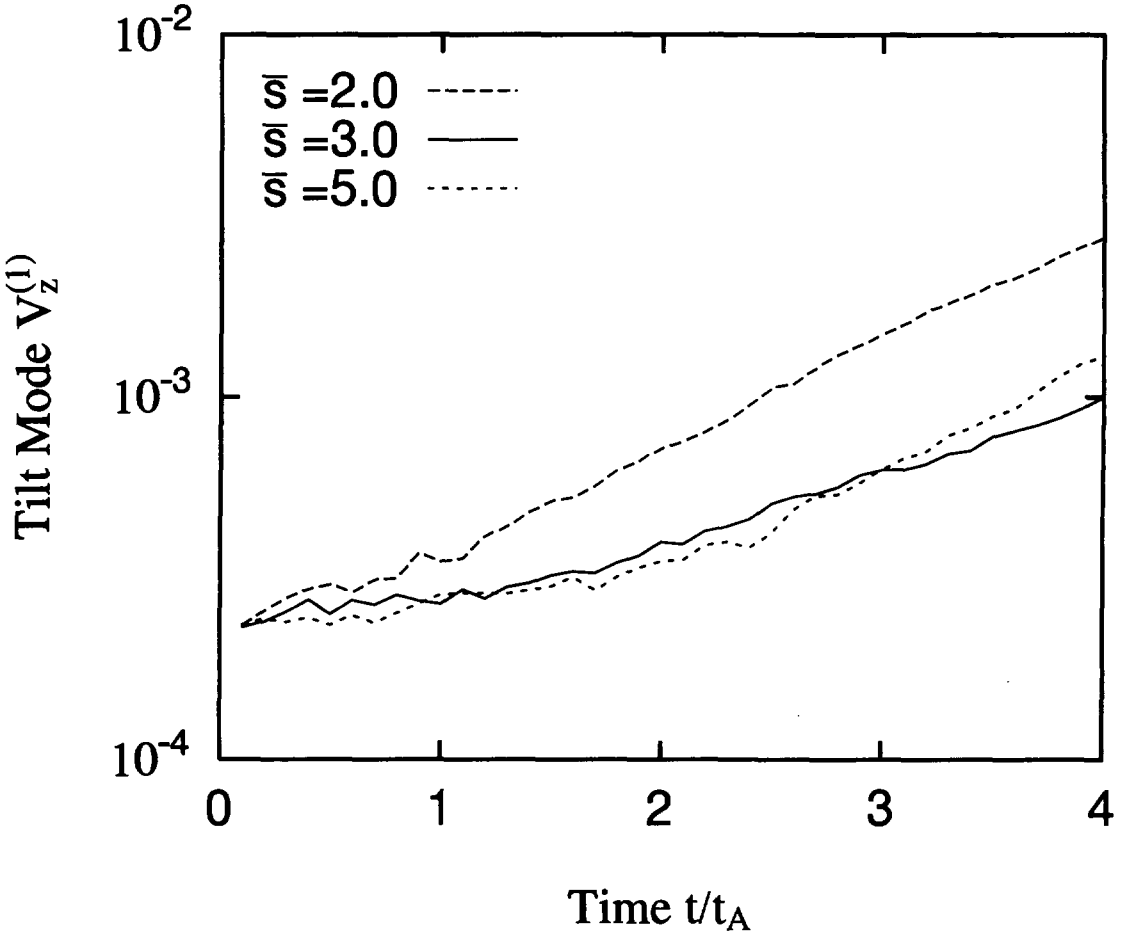
10^{-2}
10^{-3}
10^{-4}
$\bar{s}$ =2.0
$\bar{s}$ =3.0
$\bar{s}$ =5.0
Tilt Mode $V_z^{(1)}$
0
1
2
3
4
Time t/t_A

Fig.4

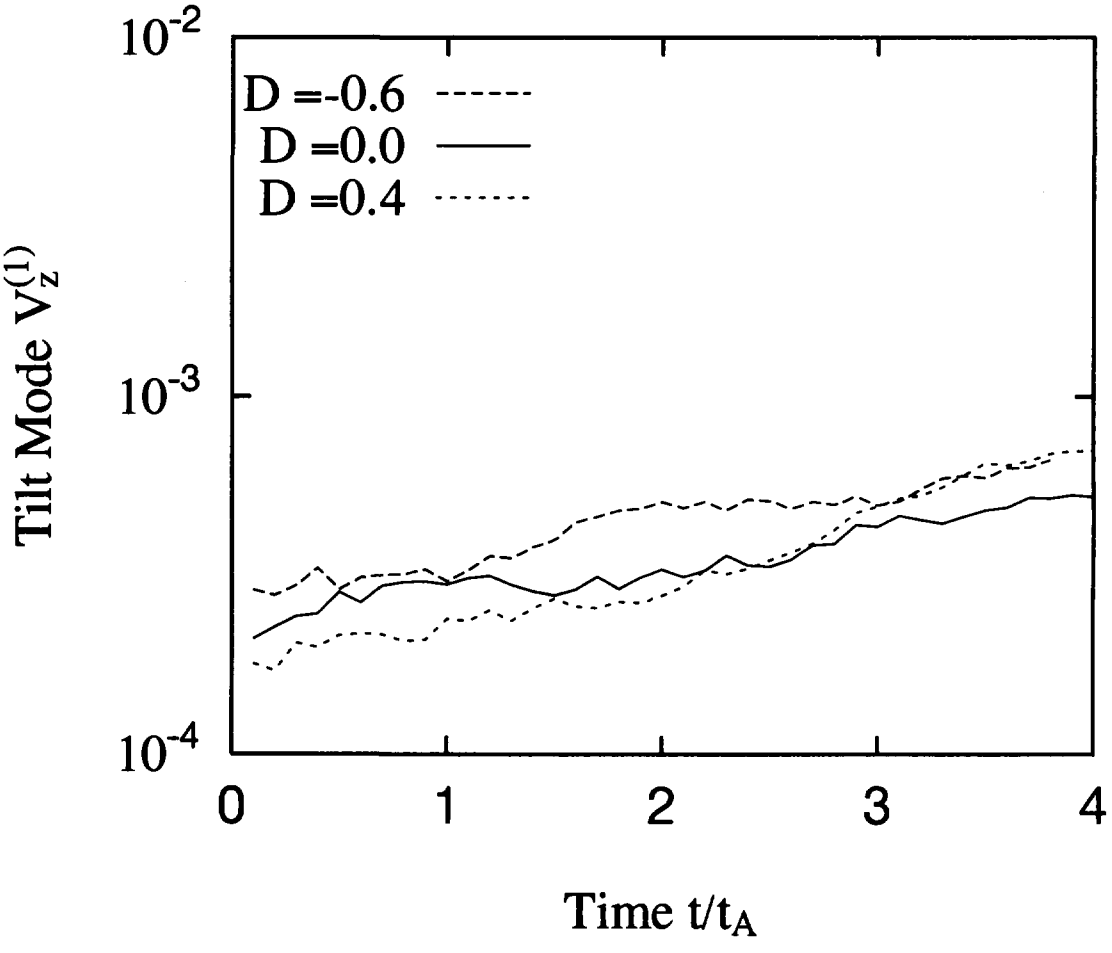

Fig.5

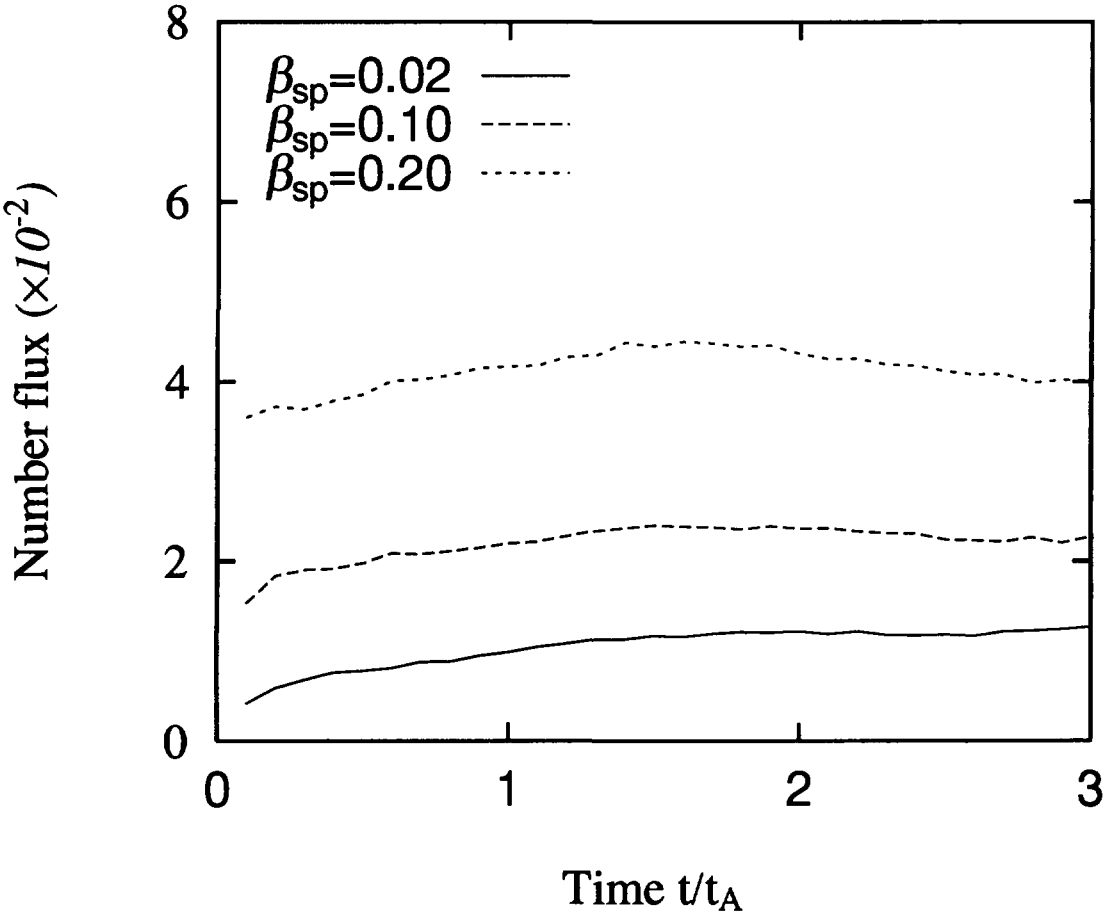
8
6
4
2
0
0
1
2
3
β_{sp}=0.02
β_{sp}=0.10
β_{sp}=0.20
Number flux ($\times 10^{-2}$)
Time t/t_A

Fig.6

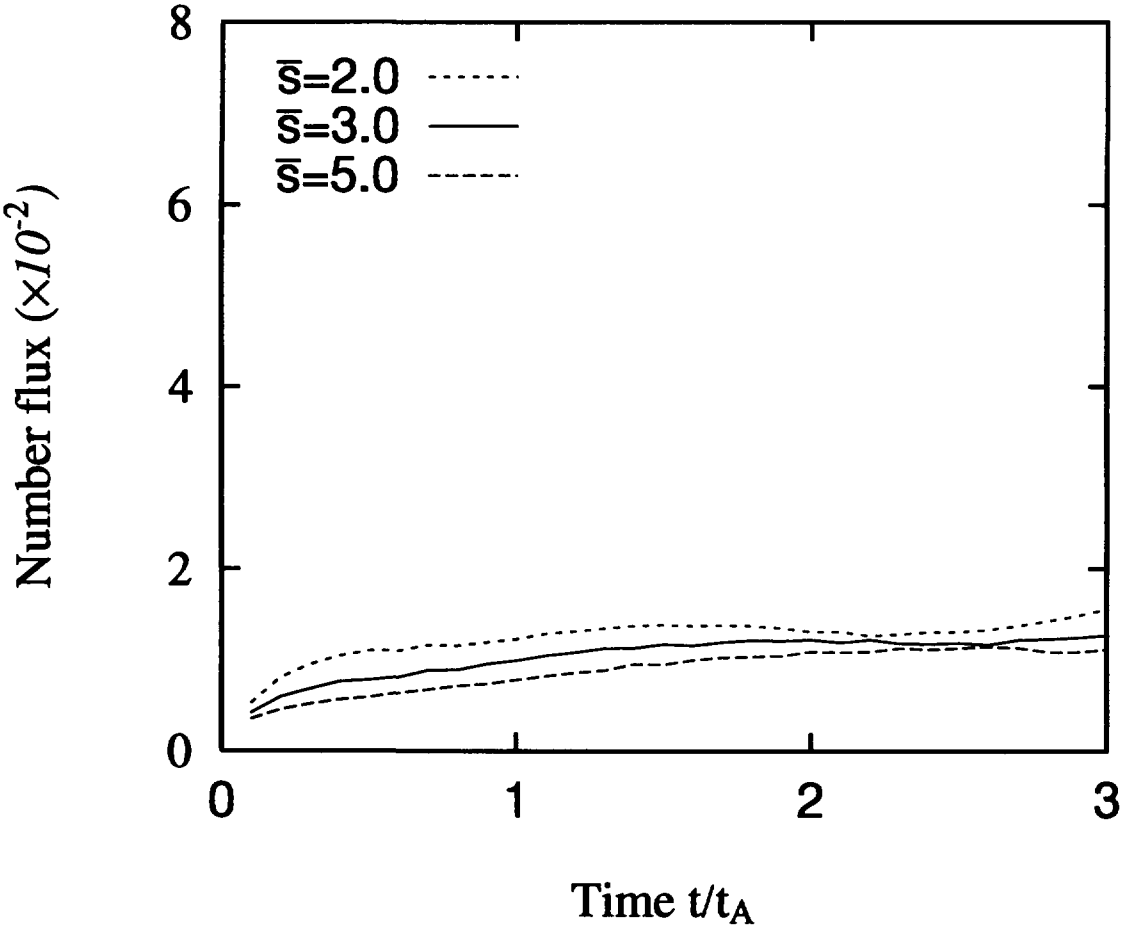

Fig.7

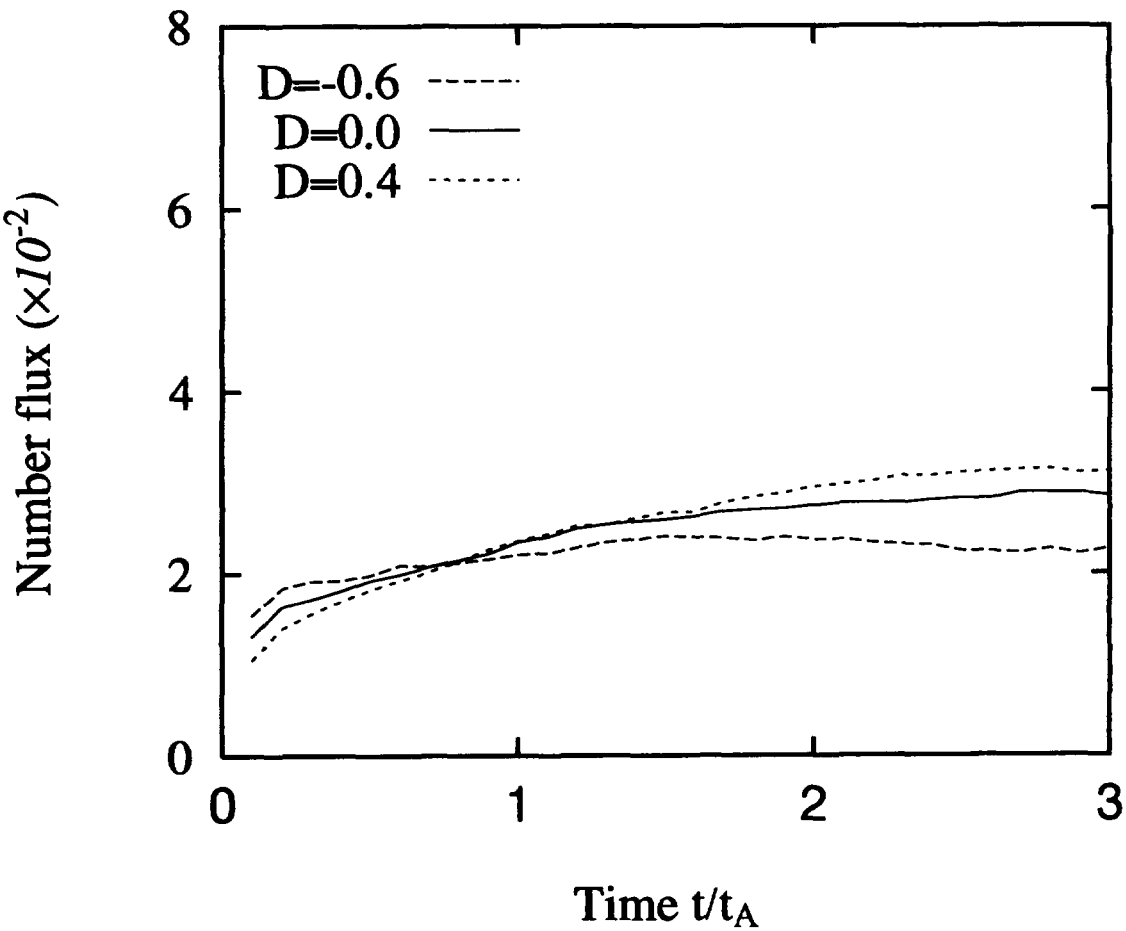

Fig.8

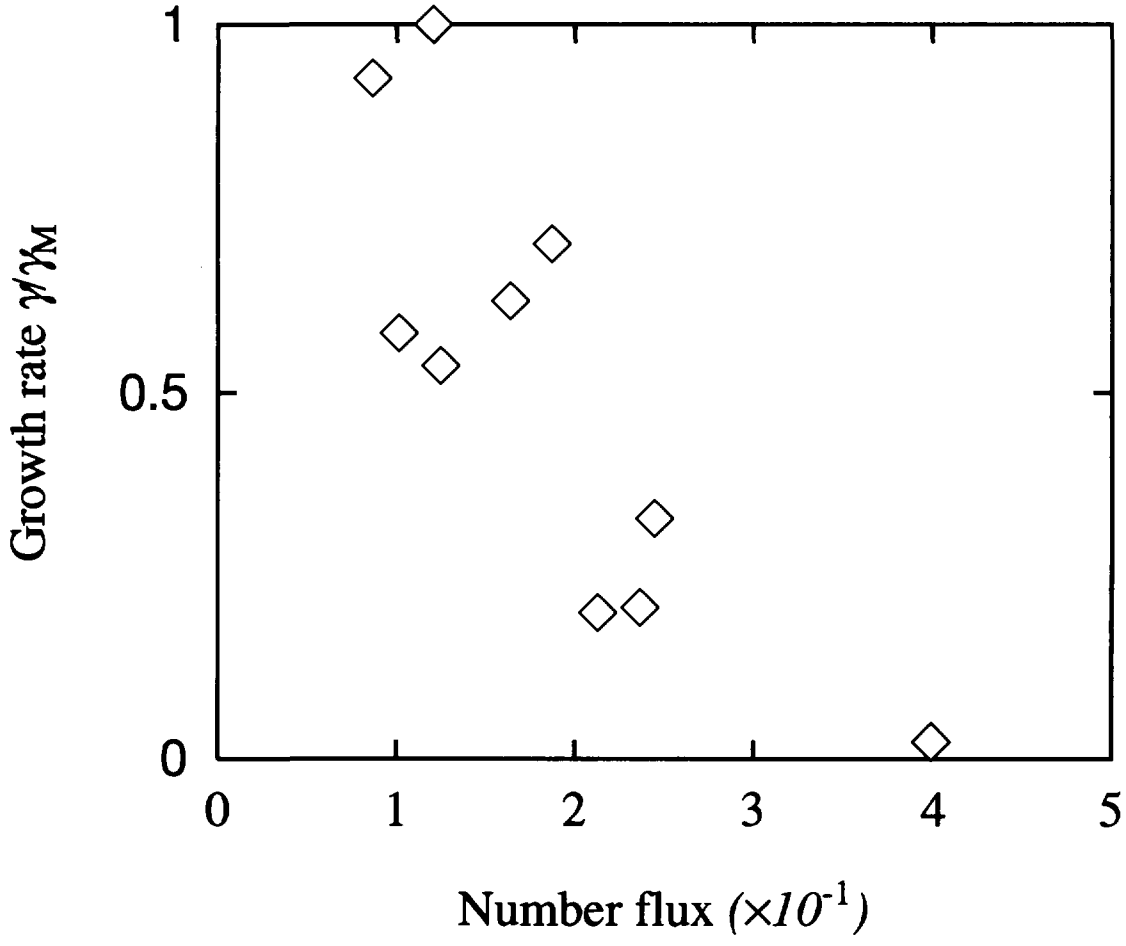

Fig.9

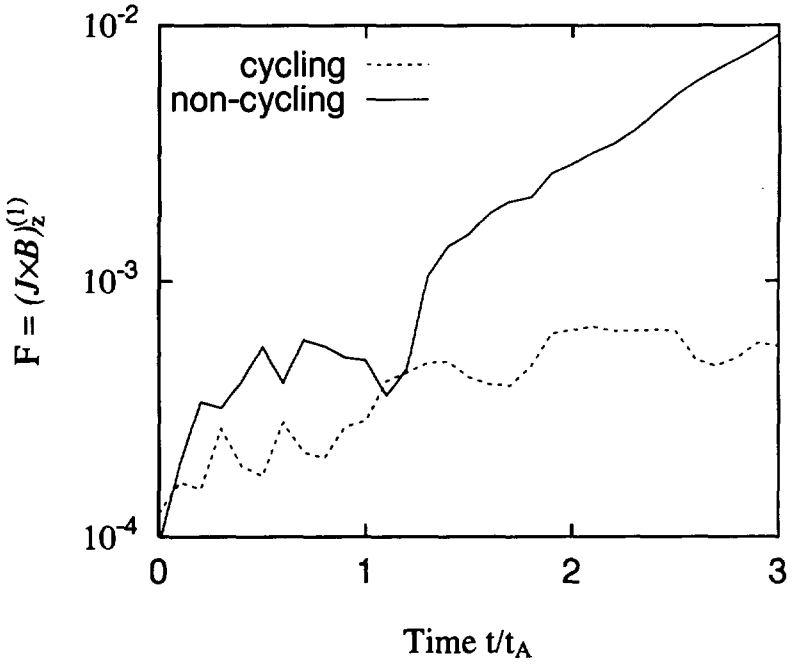
10^{-2}
10^{-3}
10^{-4}
cycling
non-cycling
$F = (J \times B)_z^{(1)}$
0
1
2
3
Time t/t_A

(a)

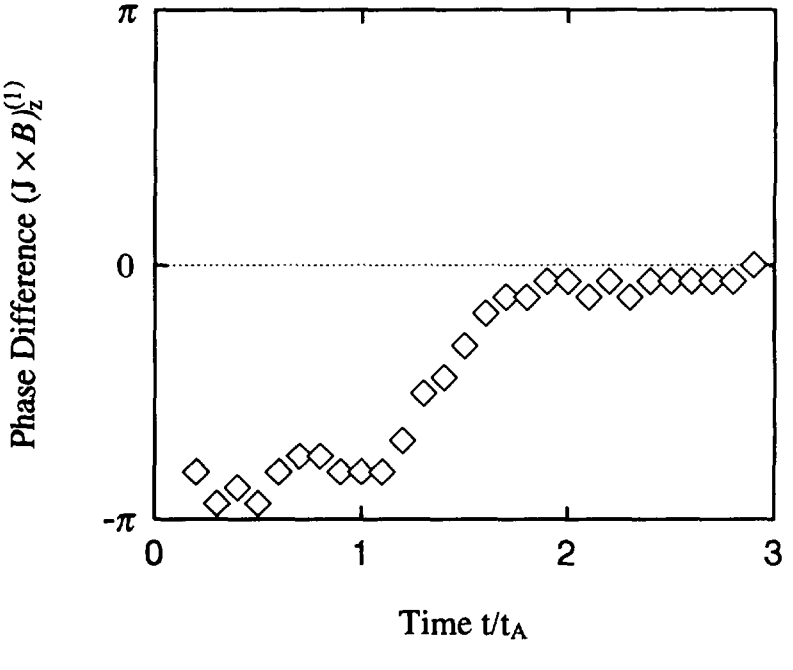
π
0
$-\pi$
Phase Difference $(J \times B)_z^{(1)}$
0
1
2
3
Time t/t_A

(b)

Fig.10

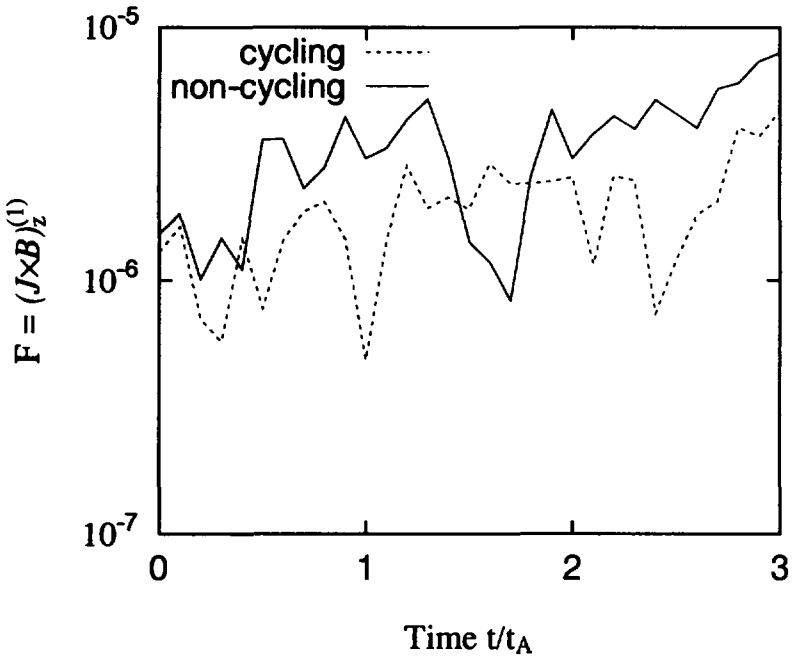
10^{-5}
10^{-6}
10^{-7}
cycling
non-cycling
$F = (J \times B)_z^{(1)}$
0
1
2
3
Time t/t_A

(a)

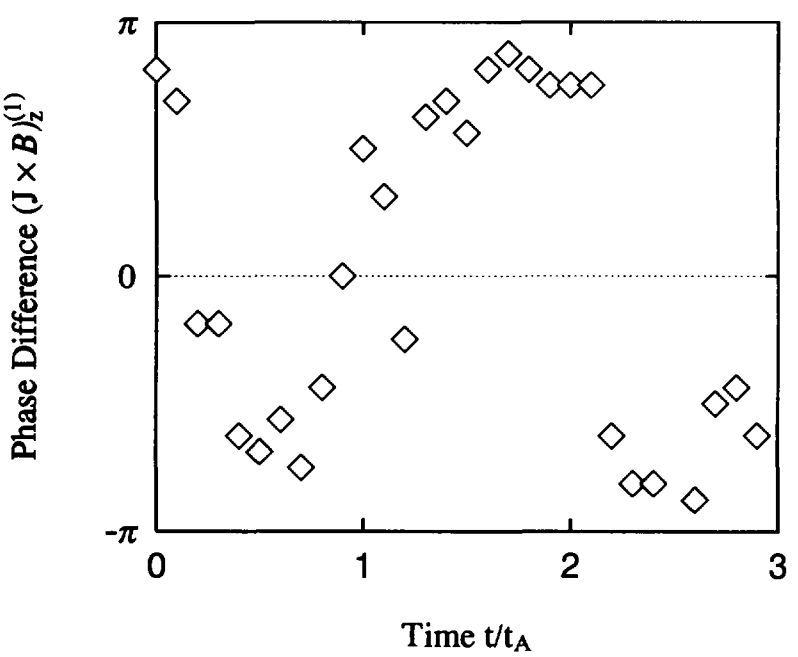
π
0
$-\pi$
Phase Difference $(J \times B)_z^{(1)}$
0
1
2
3
Time t/t_A

(b)

Fig.11

Recent Issues of NIFS Series

NIFS-448 M. Ozaki, T. Sato and the Complexity Simulation Group,
Interactions of Convecting Magnetic Loops and Arcades; Sep. 1996

NIFS-449 T. Aoki,
Interpolated Differential Operator (IDO) Scheme for Solving Partial Differential Equations; Sep. 1996

NIFS-450 D. Biskamp and T. Sato,
Partial Reconnection in the Sawtooth Collapse; Sep. 1996

NIFS-451 J. Li, X. Gong, L. Luo, F.X. Yin, N. Noda, B. Wan, W. Xu, X. Gao, F. Yin, J.G. Jiang, Z. Wu., J.Y. Zhao, M. Wu, S. Liu and Y. Han,
Effects of High Z Probe on Plasma Behavior in HT-6M Tokamak; Sep. 1996

NIFS-452 N. Nakajima, K. Ichiguchi, M. Okamoto and R.L. Dewar,
Ballooning Modes in Heliotrons/Torsatrons; Sep. 1996 (IAEA-CN-64/D3-6)

NIFS-453 A. Iiyoshi,
Overview of Helical Systems; Sep. 1996 (IAEA-CN-64/O1-7)

NIFS-454 S. Saito, Y. Nomura, K. Hirose and Y.H. Ichikawa,
Separatrix Reconnection and Periodic Orbit Annihilation in the Harper Map; Oct. 1996

NIFS-455 K. Ichiguchi, N. Nakajima and M. Okamoto,
Topics on MHD Equilibrium and Stability in Heliotron / Torsatron; Oct. 1996

NIFS-456 G. Kawahara, S. Kida, M. Tanaka and S. Yanase,
Wrap, Tilt and Stretch of Vorticity Lines around a Strong Straight Vortex Tube in a Simple Shear Flow; Oct. 1996

NIFS-457 K. Itoh, S.- I. Itoh, A. Fukuyama and M. Yagi,
Turbulent Transport and Structural Transition in Confined Plasmas; Oct. 1996

NIFS-458 A. Kageyama and T. Sato,
Generation Mechanism of a Dipole Field by a Magnetohydrodynamic Dynamo; Oct. 1996

NIFS-459 K. Araki, J. Mizushima and S. Yanase,
The Non-axisymmetric Instability of the Wide-Gap Spherical Couette Flow; Oct. 1996

NIFS-460 Y. Hamada, A. Fujisawa, H. Iguchi, A. Nishizawa and Y. Kawasumi,
A Tandem Parallel Plate Analyzer; Nov. 1996

NIFS-461 Y. Hamada, A. Nishizawa, Y. Kawasumi, A. Fujisawa, K. Narihara, K. Ida, A. Ejiri, S. Ohdachi, K. Kawahata, K. Toi, K. Sato, T. Seki, H. Iguchi, K. Adachi, S. Hidekuma, S.Hirokura, K. Iwasaki, T. Ido, M. Kojima, J. Koong, R. Kumazawa, H. Kuramoto, T. Minami, I. Nomura, H. Sakakita, M. Sasao, K.N. Sato, T. Tsuzuki, J. Xu, I. Yamada and T. Watari,
Density Fluctuation in JIPP T-IIU Tokamak Plasmas Measured by a Heavy Ion Beam Probe; Nov. 1996

NIFS-462 N. Katsuragawa, H. Hojo and A. Mase,
Simulation Study on Cross Polarization Scattering of Ultrashort-Pulse Electromagnetic Waves; Nov. 1996

NIFS-463 V. Voitsenya, V. Konovalov, O. Motojima, K. Narihara, M. Becker and B. Schunke,
Evaluations of Different Metals for Manufacturing Mirrors of Thomson Scattering System for the LHD Divertor Plasma; Nov. 1996

NIFS-464 M. Pereyaslavets, M. Sato, T. Shimozuma, Y. Takita, H. Idei, S. Kubo, K. Ohkubo and K. Hayashi,
Development and Simulation of RF Components for High Power Millimeter Wave Gyrotrons; Nov. 1996

NIFS-465 V.S. Voitsenya, S. Masuzaki, O. Motojima, N. Noda and N. Ohyabu,
On the Use of CX Atom Analyzer for Study Characteristics of Ion Component in a LHD Divertor Plasma; Dec. 1996

NIFS-466 H. Miura and S. Kida,
Identification of Tubular Vortices in Complex Flows; Dec. 1996

NIFS-467 Y. Takeiri, Y. Oka, M. Osakabe, K. Tsumori, O. Kaneko, T. Takanashi, E. Asano, T. Kawamoto, R. Akiyama and T. Kuroda,
Suppression of Accelerated Electrons in a High-current Large Negative Ion Source; Dec. 1996

NIFS-468 A. Sagara, Y. Hasegawa, K. Tsuzuki, N. Inoue, H. Suzuki, T. Morisaki, N. Noda, O. Motojima, S. Okamura, K. Matsuoka, R. Akiyama, K. Ida, H. Idei, K. Iwasaki, S. Kubo, T. Minami, S. Morita, K. Narihara, T. Ozaki, K. Sato, C. Takahashi, K. Tanaka, K. Toi and I. Yamada,
Real Time Boronization Experiments in CHS and Scaling for LHD; Dec. 1996

NIFS-469 V.L. Vdovin, T.Watari and A. Fukuyama,
3D Maxwell-Vlasov Boundary Value Problem Solution in Stellarator Geometry in Ion Cyclotron Frequency Range (final report); Dec. 1996

NIFS-470 N. Nakajima, M. Yokoyama, M. Okamoto and J. Nührenberg,
Optimization of M=2 Stellarator; Dec. 1996

NIFS-471 A. Fujisawa, H. Iguchi, S. Lee and Y. Hamada,
Effects of Horizontal Injection Angle Displacements on Energy Measurements with Parallel Plate Energy Analyzer; Dec. 1996

NIFS-472 R. Kanno, N. Nakajima, H. Sugama, M. Okamoto and Y. Ogawa,
Effects of Finite-β and Radial Electric Fields on Neoclassical Transport in the Large Helical Device; Jan. 1997

NIFS-473 S. Murakami, N. Nakajima, U. Gasparino and M. Okamoto,
Simulation Study of Radial Electric Field in CHS and LHD; Jan. 1997

NIFS-474 K. Ohkubo, S. Kubo, H. Idei, M. Sato, T. Shimozuma and Y. Takita,
Coupling of Tilting Gaussian Beam with Hybrid Mode in the Corrugated Waveguide; Jan. 1997

NIFS-475 A. Fujisawa, H. Iguchi, S. Lee and Y. Hamada,
Consideration of Fluctuation in Secondary Beam Intensity of Heavy Ion Beam Prove Measurements; Jan. 1997

NIFS-476 Y. Takeiri, M. Osakabe, Y. Oka, K. Tsumori, O. Kaneko, T. Takanashi, E. Asano, T. Kawamoto, R. Akiyama and T. Kuroda,
Long-pulse Operation of a Cesium-Seeded High-Current Large Negative Ion Source; Jan. 1997

NIFS-477 H. Kuramoto, K. Toi, N. Haraki, K. Sato, J. Xu, A. Ejiri, K. Narihara, T. Seki, S. Ohdachi, K. Adati, R. Akiyama, Y. Hamada, S. Hirokura, K. Kawahata and M. Kojima,
Study of Toroidal Current Penetration during Current Ramp in JIPP T-IIU with Fast Response Zeeman Polarimeter; Jan., 1997

NIFS-478 H. Sugama and W. Horton,
Neoclassical Electron and Ion Transport in Toroidally Rotating Plasmas; Jan. 1997

NIFS-479 V.L. Vdovin and I.V. Kamenskij,
3D Electromagnetic Theory of ICRF Multi Port Multi Loop Antenna; Jan. 1997

NIFS-480 W.X. Wang, M. Okamoto, N. Nakajima, S Murakami and N. Ohyabu,
Cooling Effect of Secondary Electrons in the High Temperature Divertor Operation; Feb. 1997

NIFS-481 K. Itoh, S.-I. Itoh, H. Soltwisch and H.R. Koslowski,
Generation of Toroidal Current Sheet at Sawtooth Crash; Feb. 1997

NIFS-482 K. Ichiguchi,
Collisionality Dependence of Mercier Stability in LHD Equilibria with Bootstrap Currents; Feb. 1997

NIFS-483 S. Fujiwara and T. Sato,
Molecular Dynamics Simulations of Structural Formation of a Single Polymer Chain: Bond-orientational Order and Conformational Defects; Feb. 1997

NIFS-484 T. Ohkawa,
Reduction of Turbulence by Sheared Toroidal Flow on a Flux Surface; Feb. 1997

NIFS-485 K. Narihara, K. Toi, Y. Hamada, K. Yamauchi, K. Adachi, I. Yamada, K. N. Sato, K. Kawahata, A. Nishizawa, S. Ohdachi, K. Sato, T. Seki, T. Watari, J. Xu, A. Ejiri, S. Hirokura, K. Ida, Y. Kawasumi, M. Kojima, H. Sakakita, T. Ido, K. Kitachi, J. Koog and H. Kuramoto,
Observation of Dusts by Laser Scattering Method in theJIPPT-IIU Tokamak Mar. 1997

NIFS-486 S. Bazdenkov, T. Sato and The Complexity Simulation Group,
Topological Transformations in Isolated Straight Magnetic Flux Tube; Mar. 1997

NIFS-487 M. Okamoto,
Configuration Studies of LHD Plasmas; Mar. 1997

NIFS-488 A. Fujisawa, H. Iguchi, H. Sanuki, K. Itoh, S. Lee, Y. Hamada, S. Kubo, H. Idei, R. Akiyama, K. Tanaka, T. Minami, K. Ida, S. Nishimura, S. Morita, M. Kojima, S. Hidekuma, S.-I. Itoh, C. Takahashi, N. Inoue, H. Suzuki, S. Okamura and K. Matsuoka,
Dynamic Behavior of Potential in the Plasma Core of the CHS Heliotron/Torsatron; Apr. 1997

NIFS-489 T. Ohkawa,
Pfirsch - Schlüter Diffusion with Anisotropic and Nonuniform Superthermal Ion Pressure; Apr. 1997

NIFS-490 S. Ishiguro and The Complexity Simulation Group,
Formation of Wave-front Pattern Accompanied by Current-driven Electrostatic Ion-cyclotron Instabilities; Apr. 1997

NIFS-491 A. Ejiri, K. Shinohara and K. Kawahata,
An Algorithm to Remove Fringe Jumps and its Application to Microwave Reflectometry; Apr. 1997

NIFS-492 K. Ichiguchi, N. Nakajima, M. Okamoto,
Bootstrap Current in the Large Helical Device with Unbalanced Helical Coil Currents; Apr. 1997

NIFS-493 S. Ishiguro, T. Sato, H. Takamaru and The Complexity Simulation Group,
V-shaped dc Potential Structure Caused by Current-driven Electrostatic Ion-cyclotron Instability; May 1997

NIFS-494 K. Nishimura, R. Horiuchi and T. Sato,
Tilt Stabilization by Energetic Ions Crossing Magnetic Separatrix in Field-Reversed Configuration; June 1997